Topological Analysis of the Electronic Charge Density in the Ethene Protonation Reaction Catalyzed by Acidic Zeolite

M. Fernanda Zalazar[†,‡] and Nélida M. Peruchena*[,†,‡]

Laboratorio de Estructura Molecular y Propiedades, Area de Química Física, Departamento de Química, Facultad de Ciencias Exactas, Naturales y Agrimensura, Universidad Nacional del Nordeste, Avda Libertad 5460, (3400) Corrientes, Argentina, and Facultad Regional Resistencia, Universidad Tecnologica Nacional, French 414 Resistencia, Chaco

Received: February 28, 2007; In Final Form: May 21, 2007

In the present work, the distribution of the electronic charge density in the ethene protonation reaction by a zeolite acid site is studied within the framework of the density functional theory and the atoms in molecules (AIM) theory. The key electronic effects such as topological distribution of the charge density involved in the reaction are presented and discussed. The results are obtained at B3LYP/6-31G** level theory. Attention is focused on topological parameters such as electron density, its Laplacian, kinetic energy density, potential energy density, and electronic energy density at the bond critical points (BCP) in all bonds involved in the interaction zone, in the reactants, π-complex, transition state, and alkoxy product. In addition, the topological atomic properties are determined on the selected atoms in the course of the reaction (average electron population, $N(\Omega)$, atomic net charge, $q(\Omega)$, atomic energy, $E(\Omega)$, atomic volume, $v(\Omega)$, and first moment of the atomic charge distribution, $M(\Omega)$) and their changes are analyzed exhaustively. The topological study clearly shows that the ethene interaction with the acid site of the zeolite cluster, T5-OH, in the ethene adsorbed, is dominated by a strong O−H$\cdots\pi$ interaction with some degree of covalence. AIM analysis based on DFT calculation for the transition state (TS) shows that the hydrogen atom from the acid site in the zeolitic fragment is connected to the carbon atom by a covalent bond with some contribution of electrostatic interaction and to the oxygen atom by closed shell interaction with some contribution of covalent character. The C−O bond formed in the alkoxy product can be defined as a weaker shared interaction. Our results show that in the transition state, the dominant interactions are partially electrostatic and partially covalent in nature, in which the covalent contribution increases as the concentration and accumulation of the charge density along the bond path between the nuclei linked increases.

Introduction

The acidic zeolites are used as catalysts for many hydrocarbon transformation reactions. The activity of these catalysts is based on the Brønsted acid site for its ability to donate a proton to a hydrocarbon that is transformed into a carbocation.[1] The term carbocation includes various groups of compounds of different structures with a positively charged carbon atom.[2] Protonation of a π bond of an alkene or an aromatic molecule creates a carbenium ion, in which a carbon atom has an empty p orbital and an electronic sextet. On the other hand, protonation of a C−C or C−H σ bond of an alkane molecule conceptually releases a carbonium ion, in which a three center two electron bond, 3c-2e, is formed preserving the electronic octet of the carbon atom.[2]

It has been widely accepted that carbonium ions play a dominant role in paraffin cracking since they are the initiators of cracking the chain proceeding via complex ionic mechanisms. In addition, the alkyl carbenium ions are involved in the chain propagation, skeletal and double bond isomerization, and alkylation and oligomerization reactions in olefins.[3] In accordance with the classification of Olah,[2] carbonium ions contain 4- or 5-fold coordinate positively charged carbon atoms. The simplest example of this type is the methonium ion (CH_5^+),[4] considered the prototype of nonclassical carbocations and hypercoordinated carbon species. Nevertheless, an intensive debate has been registered in the last years over their structure.[5] However, in carbenium ions the positive charge is sited on a 3-fold coordinate carbon atom. This group includes alkyl carbenium ions formed, e.g., by interaction of alkenes with protons and alkenyl carbenium ions generated by interaction of protons and conjugated dienes or by hydride ion abstraction from olefins by Lewis acids. The carbocation mechanism of acid catalyzed organic reactions was originally formulated and developed for homogeneous catalysis in superacidic media and later used for heterogeneous catalysis by zeolites.[6] However, the role of carbenium ions in zeolite catalyzed hydrocarbon reactions is still a question of debate,[7,8] since several studies demonstrate that small protonated olefins do not exist as free carbenium ions but rather as alkoxides bound to the zeolitic fragment.[6,7,9−12,15−18]

The interaction of small alkenes with zeolite Brønsted acid sites has been the object of several quantum chemical studies from the pioneering work of Kazansky et al.[12] The protonation of an olefin by an acid hydroxyl group results in formation of a more stable covalent alkoxide product, in which the process is concerted and occurs through a transition state, wherein the

* To whom correspondence should be addressed. E-mail: peruchen@exa.unne.edu.ar.
† Universidad Nacional del Nordeste.
‡ Universidad Tecnologica Nacional.

10.1021/jp071659v CCC: $37.00
Published on Web 07/20/2007

organic fragment resembles that of a classical carbenium ion according to these authors. Within the cluster approach, a small fragment is used to simulate the Brønsted acidic site. The cluster approach is well suited to describe local phenomena such as the interactions of molecules with active sites or the bond breaking and the bond formation processes because it allows the use of correlated methods.[7,8] However, it is recognized that structure-specific effects and effects caused by the electrostatic field present in the zeolite micropores are not well described.[19]

In this work, an atom cluster model (22 atoms) containing five tetrahedral atoms (denoted T5-OH) has been used to represent the zeolite catalyst. The same or similar clusters have been used by several workers to model reactions as the ones described here: protonation of alkenes,[7,12−15] interaction of methanol with acid zeolite,[20] interaction of methane[21] and ethane[22] with acid zeolite, dehydrogention reaction of isobutane,[23] methylation of alkenes[24] and methylbenzenes[25] by methanol and halomethanes,[26] and also the dimerization of alkenes[27] have been investigated.

Beyond the cluster approach, some workers use larger clusters combining quantum mechanics/molecular mechanics (QM/MM) methods or periodic calculations to understand the nature of the bonds in the reaction mechanism between the alkenes and the catalyst.[8,10,11,17,18,28] Generally, the quantum mechanic calculations made at different levels are based on structural and energetic parameters for the different species involved in the course of the reaction. In some cases it is accomplished with a population analysis or by Mulliken charge.[8,9,27]

Nevertheless, a study centered in the distribution of the electronic charge density, even in cluster approximation, can be of great use for these questions, especially the ones about stabilization/destabilization of the different species involved in the reactions. The apparent absence of theoretical studies on the electronic distribution in reactants, transition states, and alkoxy products in alkene protonation reactions led us to carry out a quantum chemistry ab initio investigation over the topology characteristic of the electronic distribution in the course of the protonation reaction of ethene, aiming to acquire a better understanding of the nature of the bonds involved in the transition state and in the formation product. In addition, it is interesting to have in mind that the alkene protonation is an elementary reaction present in many zeolite-catalized hydrocarbon transformations[29] (dimerization and oligomerization of olefins and double bond isomerizations, etc.), and a deep knowledge of the electronic structure of the carbocationic species is essential in order to understand the mechanisms that occur during the catalytic process.

In previous works,[30−32] we have analyzed the topological distribution of the charge density in protonated species of propane, *n*-butane, and *i*-butane and their van der Waals complexes. This analysis has been used in order to establish a relationship among the parameters that determine the stability order found for the different species and relate them to the carbonium ions structure. In all cases we found that a better understanding of the relative stabilities of the protonated *n*-butane and *i*-butane is obtained when the topological properties at the bond critical points on the distribution of the electronic charge density in the 3c-2e bonds and in their neighboring bonds are considered. These studies showed that the protonated species stability (both C-carbonium and H-carbonium ions) depends fundamentally on the way in which the cationic charge is delocalized around the neighboring bonds at the 3c-2e bonds. These results agree with the idea that the species achieve their stabilization through the positive charge distribution of the proton onto the sigma bonds.

Bear in mind that previous studies realized on several different Brønsted acid sites of zeolites[7,8] have established that the stability of the alkoxide complexes formed in the protonation reactions are very sensitive to the local geometry of the active sites; thus, from an electronic point of view, this fact must be related to the possibility of delocalization of the positive charge by the carbocation and to its capacity to interact with sites of electronic high density within the catalyst.

Therefore, it is concluded that a deep knowledge of the electronic structure of the carbocationic species in the active site of the catalyst is essential in order to understand the mechanisms that occur during the catalytic process in the alkenes transformation. In this work we present the results derived from a topology study of the electronic charge density distribution, within the framework of the atoms in molecules theory,[33] in order to investigate in depth not only what changes occur in the formation and breaking of bonds but also the ionic or covalent nature of the current atomic interactions. In addition, the role of the neighboring atoms in the redistribution of the electronic charge and in the stabilization of the alkoxy product can be investigated in this same way. On the other hand, the study of the distribution or redistribution of the electron density associated with the formation of the chemical bonds between atoms is based on a real physical property of the system and is molecular orbital independent, not employing any arbitrary charge. In this work, it is performed on species in which the experimental determinations of charge density are practically impossible, reinforcing the importance of performing this sort of study.

Method and Calculation Details

The zeolite catalyst has been modeled by a widely used cluster consisting of five tetrahedral atoms, i.e., four silicon and one aluminum atom to generate the acidic site, whose dangling bonds (which connect the cluster with the rest of the solid) are saturated with hydrogen atoms, $H_3Si-OH-Al(-O-SiH_3)_3$, denoted T5-OH.

The geometries of all species were optimized without any constraint, except for the Si−H distances mentioned above which are kept fixed at 1.42 Å, in accordance with other authors.[34] Hybrid density-functional theory calculations at the Becke3 Lee−Yang−Parr (B3LYP) level[35] with the 6-31G** basis set were carried out with the Gaussian03 suite of programs.[36] Geometrical variables were optimized using the Berny analytical gradient method.[37] All stationary points were characterized by calculating the Hessian matrix and analyzing the vibrational normal modes. Zero-point vibrational corrections (ZPE) obtained from frequency calculations were added to the total energies. For the transition state, the only normal mode corresponding to the imaginary frequency was visualized to confirm that they indeed correspond to the expected motion of atoms. In addition, calculations based on the internal reaction coordinate (IRC)[38,39] were carried out in order to investigate the minima connected by the transition state.

Topological analysis of the electron charge density was carried out using the AIMPAC[40] package of programs, and the Aim2000 package[41] was used to display molecular graphs and relief maps. The evaluation of the atomic properties were carried out with the PROAIM[42] program using the wave functions obtained at the B3LYP/6-31G** level. Also, the natural charges were obtained by natural population analysis, NPA,[43] as implemented in the Gaussian03 package of programs.[36]

Overview of Atoms in Molecules. Here, we only present the essential theoretical information that is needed for the

discussion of the numerical and graphical results, because the use of topological concepts is well documented in the standard literature.[33,44] AIM analysis is based on the critical points (CP) of the electronic density distribution. The gradient vector of the charge density vanishes in these points which are characterized by the three eigenvalues (λ_1, λ_2, and λ_3) of the Hessian matrix of the charge density ($\rho(r)$).

In the topological distribution of the electronic charge density, three topological features or elements appear as a consequence of the interaction between two atoms: (a) a bond critical point (BCP), (b) a bond path (BP), and (c) an interatomic surface (IAS).

A BCP has two negative eigenvalues and a positive eigenvalue; the two negative eigenvalues of the Hessian matrix (λ_1 and λ_2) measure the degree of contraction of the charge density at a BCP (ρ_b) perpendicular to the bond toward the critical point, while the positive eigenvalue (λ_3) measures the degree of contraction parallel to the bond and from the BCP toward each of the neighboring nuclei.

As mentioned above, the eigenvectors associated with the eigenvalue λ_3 define a unique pair of trajectories of $\nabla\rho(r)$ that originate in BCP, each of which terminates at the nucleus of one of the neighboring atoms. This pair of trajectories defines a line through space along which the electron density is a maximum with respect to any neighboring line forming an atomic interaction line (AIL) or bond path. Each bond path is homeomorphically mirrored by a virial path, a line of maximum negative potential energy density linking the same nuclei. Thus, the presence of a bond path and its associated virial path provide a universal indicator of bonding between the atoms so linked.[45]

On the other hand, an atomic surface $S(A)$ for atom A is composed of a number of interatomic surfaces $S(A|B)$, one for each bonded atom B. An interatomic surface is defined by the gradient vectors of $\rho(r)$. The set of trajectories of $\nabla\rho(r)$ that end at a BCP, define the interatomic surface that separates the basins of the neighboring atoms. Since the surface is defined by $\nabla\rho(r)$ trajectories that end at a point, and since trajectories never cross, an interatomic surface is one of zero-flux in the gradient vector field of the density. Each basin is bounded by one or more surfaces of zero flux in $\nabla\rho(r)$, some of which may occur at ∞. Thus, an atom in a molecule may be alternatively defined as a region of space bounded by one or more zero-flux surfaces.

In the AIM theory context, the identification of an atom in a molecule as an open quantum system and the criterion for bonding are inseparable, both being physical consequences of the topology of the charge density displayed at a BCP or (3,−1) CP, an ever present feature of charge distributions.[46]

On the other hand, the Laplacian of $\rho(r)$ also appears in the local expression of the virial theorem which can be written as

$$h^2/4m\nabla^2\rho(r) = 2G(r) + V(r)$$

where $G(r)$ and $V(r)$ are the kinetic and potential energy densities. Since $G(r) > 0$ and $V(r) < 0$, the potential energy dominates to the total energy in those regions of space with concentration of electronic charge, where $\nabla^2\rho_b < 0$, while the kinetic energy is dominant in regions where $\nabla^2\rho_b > 0$. Thus, a positive $\nabla^2\rho$ at a BCP reveals that the kinetic energy contribution is greater than that of potential energy and shows depletion of electronic charge along the bond path. This is the case encountered in closed shell (electrostatic) interactions.[33]

However, the density of the total electronic energy function is related to the density of the potential and kinetic energy by the expression

$$E_e(r) = G(r) + V(r)$$

where $E_e(r)$ designs the density of the total electronic energy at the r point. Calculated properties at the BCP are labeled with the subscript "b" throughout the work.

It is necessary to have in mind that bonds with covalent character must have a BCP with negative values for $\nabla^2\rho_b$ and $E_{e(b)}$; but the condition in which $|V(r)|/G(r) > 1$ but $|V(r)| < 2G(r)$ give a result such that $\nabla^2\rho_b$ would be positive (closed shell interaction), while $E_{e(b)}$ is negative (shared interaction). Therefore, they must be termed as partially covalent and partially electrostatic.[47]

In addition, the relief map of the Laplacian function for the atomic system exhibits a shell of charge concentration and another one of charge depletion for each quantum shell. The outer quantum shell of an atom over $\nabla^2\rho(r) < 0$ is called valence shell charge concentration (VSCC).

Topologically, the extremes or critical points in the distribution of the Laplacian function of $\rho(r)$ (where $\nabla(\nabla^2\rho(r)) = 0$) are classified by their rank and signature in the same way as it is done for the CPs in the charge density. It is convenient to consider the $-\nabla^2\rho$ function for a more intuitive interpretation according to some authors.[48] Thus, a (3,−3) CP corresponds to a local maximum in $-\nabla^2\rho$ (with $\nabla^2\rho < 0$), and indicates a local electronic charge concentration (CC). For an isolated atom, the VSCC is located at a sphere where the valence electronic charge is concentrated in a maximum and uniform way. Obviously, the VS loses its uniformity when the atom is within a chemical bond, and the local maximum that is created can be considered as the physical expression of the electron pairs of the Lewis model.[33,49,50]

Results

1. Topological Local Properties. The optimized geometry of the structures **3**, **4**, and **5** corresponding to the π-complex or ethene adsorbed, the transition state, TS, and the alkoxide compound in the ethene protonation reaction are shown in Figure 1. H_a represents the proton bonding to the oxygen atom in the Brønsted acid site that is transferred during the protonation reaction. The carbon atoms in neighboring positions at acid and basic sites in the zeolite cluster are distinguished with C_a and C_b, respectively. The bond distances and other relevant geometric properties are included in Table 1; at the bottom, the total energies for the species **1**−**5**, E_{ads} and E_{reac}, corrected with ZPE are shown.

In Figure 2, the molecular graphs of the species involved in the mechanism of protonation of ethene are displayed. Big circles correspond to attractors attributed to positions of atoms, and small circles correspond to critical points obtained from topological analysis of the electronic density.

Several properties that can be evaluated at the bond critical point constitute very powerful tools to classify the interactions between two fragments.[33]

In Tables 2 and 3, the most significant local topological properties (ρ_b, $\nabla^2\rho_b$, the ellipticity, ϵ, $|\lambda_1|/\lambda_3$, $|V_b|/G_b$, and G_b/ρ_b) at the bond critical points (3, −1) and at the ring critical points (3, +1) (ρ_r and $\nabla^2\rho_r$) for structures **1**−**5** (corresponding to the isolated species **1** (C_2H_4) and **2** (T5-OH); ethene adsorbed, **3**, transition state, **4**, and alkoxide product, **5**) are shown.

In Table 2, it can be seen that all the Si−O and Al−O bonds are described by relatively small values of ρ_b, positive values of $\nabla^2\rho_b$, and large values of G_b/ρ_b. The relationship $|\lambda_1|/\lambda_3$ is always less than 1 for the Si−O and Al−O bonds. All these topological properties allow one to characterize the Si−O and Al−O bonds, as closed shell interactions in species **2**−**5**, that is, bonds in which ionic interactions are the dominant ones. This

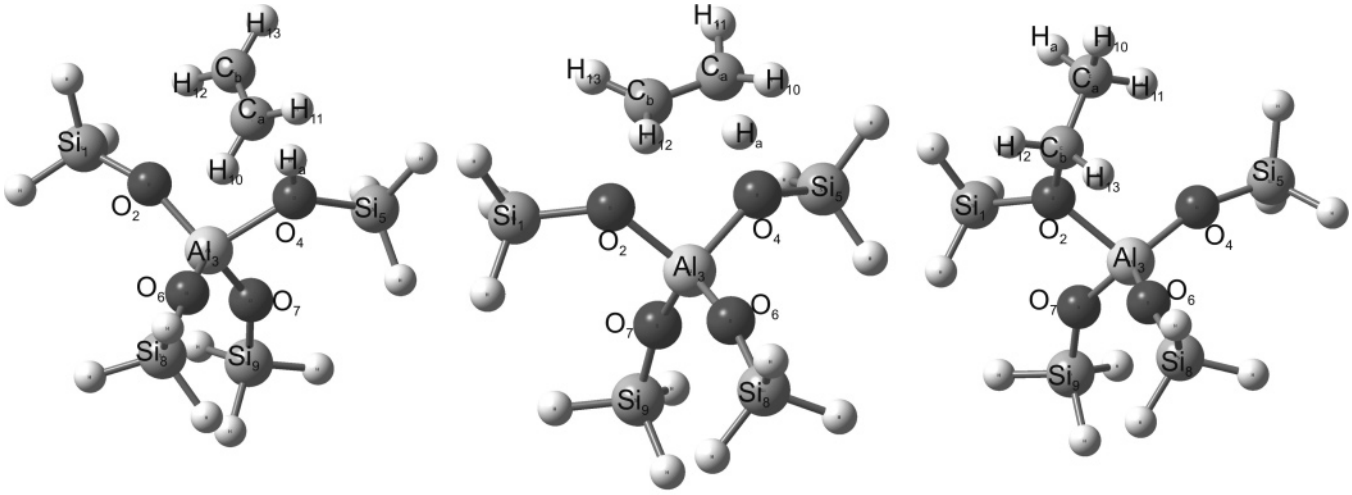

Figure 1. Optimized geometries of the structures **3**, **4**, and **5** corresponding to (a) the π-complex or ethene adsorbed; (b) the transition state, TS; and (c) the alkoxide compound in the ethene protonation reaction.

TABLE 1: Optimized Values of the Most Important Geometric Parameters[a]

	1	**2**	**3**	**4**	**5**
			Distance (Å)		
Si_1-O_2		1.642	1.637	1.671	1.734
Al_3-O_2		1.727	1.722	1.804	1.921
Al_3-O_4		1.946	1.917	1.819	1.718
Si_5-O_4		1.734	1.725	1.678	1.636
Al_3-O_6		1.708	1.719	1.722	1.718
Al_3-O_7		1.729	1.733	1.723	1.736
O_4-H_a		0.970	0.981	1.330	4.115
Si_8-O_6		1.635	1.635	1.634	1.636
Si_9-O_7		1.644	1.643	1.636	1.646
C_a-C_b	1.330		1.337	1.400	1.516
C_a-H_{11}	1.087		1.087	1.090	1.095
C_a-H_{10}	1.087		1.087	1.090	1.092
C_b-H_{12}	1.087		1.087	1.083	1.092
C_b-H_{13}	1.087		1.087	1.083	1.093
$C_b\cdots O_2$			3.720	2.121	1.469
$C_a\cdots H_a$			2.243	1.296	1.094
$C_b\cdots H_a$			2.232		
$H_{10}\cdots O_6$			2.974		
$H_{12}\cdots O_2$			2.854		
$H_{11}\cdots O_4$					2.794
			Bond Angles (deg)		
$H_aO_4Al_3$		105.9	116.9	104.1	
$O_4Al_3O_2$		94.0	103.2	98.3	105.1
$C_bO_2Al_3$				114.9	119.4
$Si_1O_2Al_3$		153.3	156.6	127.0	118.0
$Si_5O_4Al_3$		122.3	123.2	133.6	161.1
$C_aH_aO_4$			152.9	173.9	
$C_bH_aO_4$			153.0	135.7	
			Dihedral Angles (deg)		
$H_{10}C_aH_{11}C_b$		180.0	−179.1	−140.9	−120.7

[a] Calculated at the B3LYP/6-31G** level. (Distances in Å and angles in degrees). The total energies values corrected with ZPE are −78.542 688 au, −1709.324 616 au, −1787.876 788 au, −1787.838 852 au, and −1787.892 919 au for species **1**−**5**, respectively. The adsorption energy, $E_{ads} = -5.95$ kcal/mol, was calculated by subtracting the total energies of the reactants from the total energy of ethene adsorbed. The reaction energy $E_{reac} = -10.12$ kcal/mol (Both the adsorption and reaction energies were corrected by ZEP). These results are in accordance with results obtained by other authors.

condition does not change significantly in the course of the protonation reaction. The total electronic energy density at the BCP ($E_{e(b)}$) presents very small values for those bonds, being both positive and negative. They are analyzed later.

The topological properties at the BCP on C_a-C_b, $C_{a,b}-H$, and O_4-H_a bonds are clearly indicative of shared interactions, namely, a relatively large value for ρ_b and a negative value for $\nabla^2\rho_b$. The relationship $|\lambda_1|/\lambda_3$ is appreciably greater than 1, and $E_{e(b)}$ is large and negative. Finally, the G_b/ρ_b is less than 1, but their characteristics change substantially during the reaction.

1.1. Isolated Species and Ethene Adsorbed. The most important topological changes observed by formation of the π-complex in ethene adsorbed are a new BCP on the $H_a\cdots\pi$ BP and the decrease of the electronic charge density in the BCPs, at the C_a-C_b and O_4-H_a bonds. These results are in accordance with the lengthening of both the C_a-C_b and the O_4-H_a bond lengths reported by Boronat et al.[8] Also, the Laplacian, the ellipticity, and the relations $|\lambda_1|/\lambda_3$ and G_b/ρ_b decrease smoothly. With respect to the isolated species, the electronic redistribution that accompanies the formation of the π-complex shows that the C_a-C_b bond maintains its own characteristics of a double bond ($\rho_b = 0.3436$ au and $\epsilon = 0.3557$). The C−C distance is increased slightly by 0.007 Å (1.330 Å in **1** to 1.337 Å in **3**) being observed by a diminution of the electronic density of 0.038 au that is accompanied by a diminution in the ellipticity value. The acidic hydrogen atom is practically located at the same distance from both carbon atoms of the double bond, with H_a at distances of 2.240 and 2.232 Å from C_a and C_b, respectively. The topological properties at the BCP for the $H_a\cdots\pi$ interaction show that this interaction corresponds to a closed shell one, and it constitutes a clear indicator of the formation of the $O-H\cdots\pi$ complex. Nevertheless, it is interesting to emphasize that the values of the ρ_b (0.020 au) are greater than the reported ones for other $O-H\cdots\pi$ interactions by Novoa et al.[51] (0.011 au for the C_2H_4/H_2O complex and 0.007 au for the C_6H_6/H_2O complex). Also, two other BCPs corresponding to $C-H\cdots O$ closed shell interactions are encountered, where two hydrogen atoms from ethene are oriented to interact weakly with two oxygen atoms of the cluster, additionally stabilizing the ethene adsorbed. Nevertheless these interactions display lower values of ρ_b (0.004 and 0.005 au) and in consequence are weaker.

In the topology of the electronic density distribution, the formation of a bond between two atoms is visualized by means of a line of maximum density linking the nuclei of the two atoms. Note that this line is formed by two trajectories that are originated in the BCP and each of which terminates at a nucleus

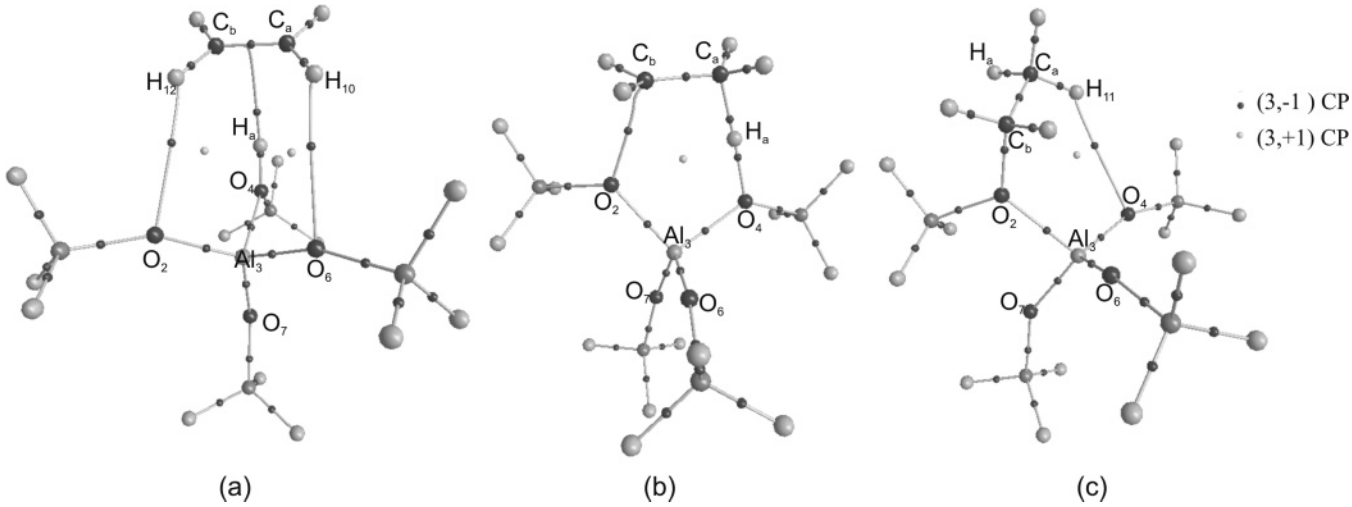

Figure 2. Molecular graphs for (a) ethene adsorbed, **3**; (b) transition state, **4**; and (c) alkoxy product, **5**. Big circles correspond to attractors attributed to nuclei, lines connecting the nuclei are the bond paths, and the small circles on them are the BCP. In part a, the two long and curved bond paths corresponding to O···H and a bond path between the H_a atom and the π-cloud, corresponding to $H_a\cdots\pi_{(CC)}$, where the H_a atom is connecting to the center of the C−C bond path with similar distance between the two carbons, is noted. In part b, it can be noted that the presence of the bond path that connects the oxygen atom neighboring (basic site) with the electronic deficient carbon atom, C_b, and the two bond paths involving the hydrogen atom, H_a, are in agreement with what was explained previously. In part c, the absence of a bond path that connects the hydrogen atom with the oxygen atom at the acid site and the presence of a C_bO_2 bond path forming the alkoxy product (see text) can be noted.

of one of the neighboring atoms. From the molecular graph (see Figure 2a), the bond paths in ethene adsorbed can be seen. The bond paths are indicated with full lines and the BCPs are indicated with full circles. In the C−H···O and $O_4-H_a\cdots\pi$ interactions, larger distances between their BCPs and the hydrogen atoms, characteristic of these weak interactions, can be seen. Also, it is important to highlight that the bond path display in Figure 2a, between the H_a atom and the π-cloud, clearly show that the H_a atom is connected to the center of the C−C bond path with similar distance between the two atoms. This situation is also encountered in the C_2H_4/H_2O complex.[51] In addition, the two C−H···O weak interactions are involved in the definition of the two rings (see Figure 2a). In the topological analysis only two ring critical points, RCPs, or (3, +1) CP are found. The topological properties in these RCPs are shown in Table 3. The CPs of the distribution satisfy the Poincaré−Hopf relation.[52]

Figure 3 shows the contour maps of the Laplacian ($\nabla^2\rho$) in the plane that contains the BCP between both carbon atoms and the hydrogen atom (H_a) of the zeolite Brønsted acid site. The $H_a\cdots\pi$ BCP lies in a zone of decrement of the electronic charge density, that is in the region of $\nabla^2\rho_b > 0$, in correspondence with a closed shell interaction. In this region (with depletion of the charge density), the projections about the plane of the two BCPs corresponding to C−H···O bonds and its bond paths can also be observed.

It is also interesting to consider the result of the topological properties at the Al−O and Si−O bonds. In the isolated cluster, the analysis of the electronic density at the BCPs in the region formed by neighboring atoms at the protonated oxygen, denoted O_4, shows some facts that differentiate and characterize the acid site. If we compare the local properties of the $Al-O_4/Si-O_4$ bonds with the other Al−O/Si−O bonds of the zeolite lattice, it can be seen that both the density and the Laplacian values are diminished, indicating an electronic distribution in the protonated zeolite cluster that weakens the bonds on the acid site. These density and Laplacian values ($\rho_b = 0.0508$ and 0.1030 au and $\nabla^2\rho_b = 0.3458$ and 0.6575 au) are in line with structural data. As it can be observed in Table 1, the $Al-O_4$ and $Si-O_4$ bond distances are 1.946 and 1.734 Å, respectively, thus indicating a lengthening in both cases.

On the other hand, a redistribution of the electronic density is also observed on all the Al−O and Si−O bonds when the π-complex is formed, being noticeable a slight increase of ρ_b and $\nabla^2\rho_b$ in two $Al-O_{2,4}/Si-O_{2,4}$ bonds and a minor diminution in the other two bonds $Al-O_{6,7}/Si-O_{6,7}$. Nevertheless in the π-complex, the bonds of the acid site maintain an appreciable minor value of density in the BCPs (0.054 au/0.105 au for $Al-O_4/Si-O_4$). This situation is reversed at the end of the reaction when the alkoxide product is formed, as it is seen later.

1.2. Transition State. Previous studies (Kazansky et al.)[12] have proposed that protonation of an olefin by an acid hydroxyl group results in formation of a more stable covalent alkoxide species. In this mechanism, the process is concerted and occurs through a transition state in which the geometry and electronic structure of the organic fragment resembles that of a classical carbenium ion where new bonds are formed and other bonds are broken or weaken.

As well as always requiring energy, the making and breaking bonds also always require an electronic redistribution, and in this process, the nature of the interactions found in this TS can undergo dramatic changes. For this reason, the information that an AIM analysis can offer about the nature of the present interactions in the TS and on the way they evolve in the course of the reaction is very useful.

The C_a-C_b bond in the transition state undergoes a transition from a double to a single bond. This situation is reflected by the curvature values of the charge density at BCP, giving as results the following values of the ellipticity: $\epsilon = 0.356$ in the adsorbed and $\epsilon = 0.194$ in the TS. Therefore, the electronic charge density is shifting toward the proton that is being transferred from the acid site. The decrease of ρ_b at the C_a-C_b and O_4-H_a bonds (in accordance with the decrease in νCC and νOH vibrational frequencies) that accompanies the formation of the π-complex continues in the transition state. However, a dramatic change in the topological properties at the O_4-H_a bond is observed.

TABLE 2: Local Topological Properties (in au.) of the Electronic Charge Density Distribution Calculated at the Position of the Bond Critical Points of Selected Bond Paths for Species 1−5[a]

species	bond	ρ_b	$\nabla^2\rho_b$	ϵ	$\lvert\lambda_1\rvert/\lambda_3$	G_b/ρ_b	$\lvert V_b\rvert/G_b$	$E_{e(b)}$
1	C_a-C_b	0.3474	−1.0213	0.3884	2.7911	0.3967	3.8527	−0.3931
	$C_{a,b}-H_{10,11,12,13}$	0.2827	−1.0102	0.0162	1.5911	0.1488	8.0027	−0.2946
2	H_a-O_4	0.3499	−2.0695	0.0111	1.1737	0.1969	9.5099	−0.5863
	Al_3-O_2	0.0897	0.7977	0.0320	0.1450	2.0855	0.9338	0.0124
	Al_3-O_4	0.0508	0.3458	0.0198	0.1530	1.5764	0.9199	0.0064
	Al_3-O_6	0.0928	0.8529	0.0272	0.1436	2.1534	0.9331	0.0134
	Al_3-O_7	0.0897	0.7939	0.0276	0.1451	2.0771	0.9353	0.0121
	Si_1-O_2	0.1271	0.9699	0.0064	0.1599	2.0891	1.0867	−0.0230
	Si_5-O_4	0.1030	0.6575	0.0652	0.1771	1.7725	1.0999	−0.0183
	Si_8-O_6	0.1284	0.9948	0.0036	0.1595	2.1168	1.0848	−0.0230
	Si_9-O_7	0.1267	0.9618	0.0116	0.1604	2.0804	1.0875	−0.0230
3	C_a-C_b	0.3436	−1.0009	0.3557	2.6452	0.3890	3.8725	−0.3839
	C_a-H_{11}	0.2836	−1.0225	0.0103	1.5910	0.1426	8.3212	−0.2961
	C_a-H_{10}	0.2850	−1.0418	0.0136	1.6090	0.1356	8.7396	−0.2991
	C_b-H_{12}	0.2852	−1.0458	0.0137	1.6130	0.1345	8.8137	−0.2998
	C_b-H_{13}	0.2835	−1.0216	0.0100	1.5900	0.1428	8.3099	−0.2959
	O_4-H_a	0.3341	−1.9502	0.0128	1.1411	0.2102	8.9430	−0.5578
	Al_3-O_2	0.0905	0.8102	0.0261	0.1448	2.0994	0.9338	0.0126
	Al_3-O_4	0.0539	0.3840	0.0367	0.1533	1.6324	0.9099	0.0079
	Al_3-O_6	0.0908	0.8182	0.0273	0.1446	2.1114	0.9329	0.0129
	Al_3-O_7	0.0886	0.7805	0.0221	0.1448	2.0656	0.9335	0.0122
	Si_1-O_2	0.1283	0.9883	0.0046	0.1591	2.1073	1.0862	−0.0233
	Si_5-O_4	0.1046	0.6842	0.0742	0.1761	1.8049	1.0939	−0.0177
	Si_8-O_6	0.1286	0.9943	0.0032	0.1590	2.1138	1.0858	−0.0233
	Si_9-O_7	0.1271	0.9680	0.0080	0.1599	2.0863	1.0871	−0.0231
	$H_a\cdots\pi$	0.0205	0.0446	0.8383	0.2880	0.5157	0.9460	0.0006
	$H_{10}\cdots O_6$	0.0037	0.0144	0.2426	0.1525	0.7371	0.6849	0.0009
	$H_{12}\cdots O_2$	0.0047	0.0178	0.1551	0.1601	0.7428	0.7349	0.0009
4	C_a-C_b	0.3091	−0.8579	0.1941	2.0743	0.3385	4.0498	−0.3191
	C_a-H_{11}	0.2768	−0.9522	0.0527	1.5718	0.1670	7.1518	−0.2843
	C_a-H_{10}	0.2758	−0.9471	0.0573	1.5711	0.1682	7.1026	−0.2832
	C_b-H_{12}	0.2956	−1.1547	0.0288	1.6931	0.1082	11.0283	−0.3207
	C_b-H_{13}	0.2953	−1.1430	0.0305	1.6801	0.1122	10.6281	−0.3189
	$H_a\cdots O_4$	0.1247	0.0112	0.0190	0.4962	0.6115	1.9633	−0.0734
	Al_3-O_2	0.0753	0.5981	0.0323	0.1519	1.8556	0.9302	0.0098
	Al_3-O_4	0.0714	0.5603	0.0284	0.1521	1.8207	0.9228	0.0100
	Al_3-O_6	0.0899	0.8093	0.0096	0.1435	2.1060	0.9309	0.0131
	Al_3-O_7	0.0898	0.8081	0.0259	0.1440	2.1054	0.9319	0.0129
	Si_1-O_2	0.1212	0.8634	0.0357	0.1658	1.9774	1.0990	−0.0237
	Si_5-O_4	0.1178	0.8344	0.0388	0.1668	1.9538	1.0936	−0.0215
	Si_8-O_6	0.1293	1.0009	0.0018	0.1589	2.1189	1.0865	−0.0237
	Si_9-O_7	0.1287	0.9913	0.0019	0.1592	2.1094	1.0871	−0.0236
	$C_b\cdots O_2$	0.0504	0.1140	0.1236	0.2457	0.6580	1.1408	−0.0047
	$C_a\cdots H_a$	0.1612	−0.3495	0.0114	0.9441	0.2261	4.3972	−0.1238
5	C_a-C_b	0.2560	−0.6205	0.0390	1.4057	0.2258	4.6829	−0.2129
	C_a-H_{10}	0.2754	−0.9426	0.0069	1.5143	0.1639	7.2182	−0.2808
	C_a-H_{11}	0.2804	−0.9874	0.0056	1.5474	0.1514	7.8159	−0.2893
	C_b-H_{13}	0.2916	−1.0914	0.0433	1.6280	0.1238	9.5581	−0.3090
	C_b-H_{12}	0.2886	−1.0537	0.0475	1.5962	0.1329	8.8669	−0.3018
	Al_3-O_2	0.0545	0.3796	0.0393	0.1550	1.6138	0.9217	0.0069
	Al_3-O_4	0.0910	0.8205	0.0287	0.1447	2.1129	0.9337	0.0128
	Al_3-O_6	0.0909	0.8213	0.0295	0.1445	2.1158	0.9329	0.0129
	Al_3-O_7	0.0881	0.7729	0.0245	0.1452	2.0569	0.9331	0.0121
	Si_1-O_2	0.1038	0.6508	0.0764	0.1789	1.7593	1.1087	−0.0198
	Si_5-O_4	0.1283	0.9908	0.0027	0.1590	2.1109	1.0857	−0.0232
	Si_8-O_6	0.1283	0.9910	0.0042	0.1592	2.1112	1.0856	−0.0232
	Si_9-O_7	0.1262	0.9560	0.0100	0.1604	2.0754	1.0872	−0.0228
	C_b-O_2	0.2166	−0.2912	0.0272	0.8966	0.9551	2.3519	−0.2797
	C_a-H_a	0.2768	−0.9478	0.0071	1.5176	0.1636	7.2322	−0.2822
	$H_{11}\cdots O_4$	0.0057	0.0213	0.2770	0.1620	0.7591	0.7690	0.0010

[a] See text and Figure 1 for an explanation of symbols and identification of atoms. The eigenvalues of the Hessian matrix of ρ at BCP in the O_4-H_a bond, in **4**, are $|\lambda_1| = 0.329$; $|\lambda_2| = 0.323$; and $\lambda_3 = 0.664$.

In one step, the hydrogen atom of the bridging hydroxyl group protonates the carbon atom of the olefin double bond, C_a, and it becomes dicoordinated, $C_a\cdots H_a\cdots O_4$. The density values at $O_4\cdots H_a$ BCP decrease from 0.3341 au in **2** to 0.1247 au in **3**.

This decrease in electronic density (between both atoms that form the $O_4\cdots H_a$ bond in the acid hydroxyl group) is caused by the decrease in the perpendicular contractions of the density toward the bond path in both directions perpendicular to the

TABLE 3: Local Topological Properties (in au) of the Electronic Charge Density Distribution Calculated at the Position of the Ring Critical Points for Species 3−5

species	ring	ρ_r	$\nabla^2\rho_r$	$\lvert\lambda_1\rvert/\lambda_3$	G_b/ρ_r	$\lvert V_r\rvert/G_r$
3	$H_a-O_4-Al_3-O_6\cdots H_{10}-C_a$	0.0029	0.0124	0.1688	0.7918	0.6539
	$H_a-O_4-Al_3-O_2\cdots H_{12}-C_b$	0.0033	0.0142	0.1827	0.8106	0.6706
4	$H_a\cdots O_4-Al_3-O_2\cdots C_b-C_a$	0.0121	0.0582	0.2031	1.0373	0.8434
5	$O_4-Al_3-O_2-C_b-C_a-H_{11}$	0.0050	0.0224	0.1730	0.8724	0.7205

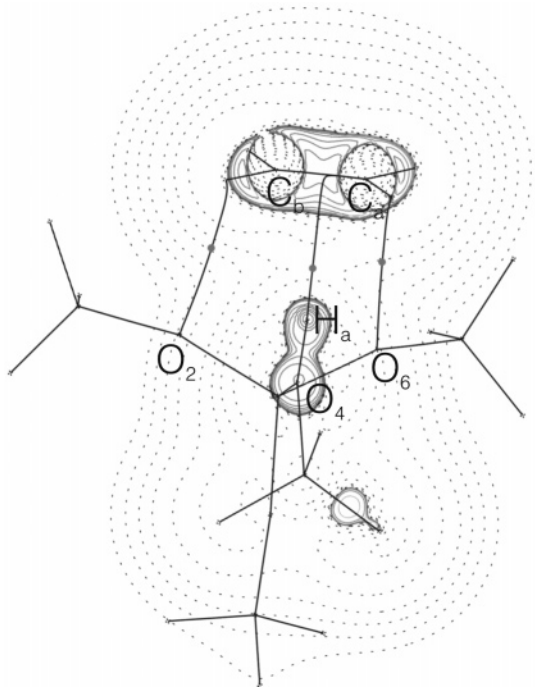

Figure 3. Contour map of the Laplacian distribution $\nabla^2\rho(r)$ and molecular graphs for ethene adsorbed, **3**, in the plane that contains the BCP between both carbon atoms and the hydrogen atom, H_a, of the zeolite Brønsted acid site. Solid lines represent regions of electronic charge concentration, and broken lines denote regions of electronic charge depletion. The contours of the $\nabla^2\rho(r)$ increase(+)/decrease(−), respectively, from the zero contour in the order $\pm 2 \times 10^{-n}$, $\pm 4 \times 10^{-n}$, $\pm 8 \times 10^{-n}$, with n beginning at 3 and decreasing in steps of unity. The molecular graph is superimposed. Lines connecting the nuclei are the bond paths; the black dots on them are the BCP.

bond trajectory. This diminution of density contraction is similar in both directions.

On the other hand, it is evident that the diminution of the density at the BCP is not due to an increase on the expansion of the ρ_b toward the path bond (associated with eigenvalue λ_3). It can be observed in the footnote of Table 2, that λ_3 does not increase but drops its value, being evident in the dominance of the expansion ($\lambda_3 = 0.664$) over the contraction of the density ($|\lambda_1| = 0.329$ and $|\lambda_2| = 0.323$) in the analyzed interaction.

With the lower ρ_b value, a positive $\nabla^2\rho_b$ value is observed in the $O_4\cdots H_a$ bond (it can be noted that $\nabla^2\rho_b$ is lower than zero for ethene adsorbed, **3**). It should be kept in mind that the Laplacian magnifies the small changes in the electron density in the bond.

In addition, the relationship between the perpendicular and parallel curvature at BCP, $|\lambda_1|/\lambda_3$, reflects the change in the topology of the density distribution (with values of 0.496 au in **4**, whereas in **3** this value is 1.141 au). Thus, it is notably lower (2.3 times lower) in the transition state than in ethene adsorbed. In regards to the energy densities, at the BCP in the TS, it can be seen that the kinetic energy density values, G_b, are slightly greater (from 0.070 to 0.076 au). Notwithstanding, the potential energy density values, V_b, in the $O_4\cdots H_a$ bond is remarkably diminished (4.2 times lower) compared with O_4-H_a bond in species **3**. As a consequence of what was pointed out above, dramatic differences on the kinetic energy density per charge unit, G_b/ρ_b, and on the relationship $|V_b|/G_b$ are found. Thus, G_b/ρ_b is approximately 3.0 times higher (0.611 vs 0.210 au), whereas $|V_b|/G_b$ is 4.5 times smaller (1.963 vs 8.943 au) in the TS than that of in species **3**. This diminution of the potential energy at BCP allows one to explain the change of the O_4-H_a bond to the $O_4\cdots H_a$ bond in the transition state for the protonation reaction in ethene.

Simultaneously, the new bond between the H_a and C_a atoms appears and a new BCP is found. This perhaps implies that the hydrogen atom is shifting between the two atoms. So the bond's nature in the TS structure is interesting, because the hydrogen atom becomes dicoordinate and lies nearly at the middle of the distance between the oxygen and carbon atoms (see Table 1 where the hydrogen atom, H_a, is localized at 1.330 Å from O_4 and 1.296 Å from C_a). In the molecular graph (Figure 2b), the presence of the new bond path that connects both atoms is noted, in agreement with what was explained previously. The $C_a\cdots H_a$ BCP is located at 0.886 Å of C_a and at 0.410 Å of H_a. The density value in this BCP is lower (0.161 au), and a less negative $\nabla^2\rho_b$ value (−0.349 au) is encountered in relation to other C−H bonds in ethene. In Table 2 it can be observed that the Laplacian value diminishes to less than half of the current values.

Nevertheless, local topological property values at the $C_a\cdots H_a$ BCP agree with usual values of a covalent bond. However, these values make it possible to distinguish differences between the $C_a\cdots H_a$ bond and the other two C_a-H bonds. The kinetic and potential energy densities are diminished, and the $|\lambda_1|/\lambda_3$ relationship is slightly lower than 1 as well. Nevertheless $|V_b|/G_b$ is quite greater than 1, although smaller than in other C_a-H bonds.

However, the local gain of the potential energy density over the kinetic energy density at the BCP corresponding to the new $C_a\cdots H_a$ bond involved in the concerted transition state is less than that in the BCPs corresponding to the other C_a-H bonds. These results are in accordance with the variation detected in the bond distances (see Table 1, C_a-C_b, O_4-H_a, C_a-H_a, and C_a-H distances). Thus, the Laplacian and the electronic energy density values are negative and, in consequence, the $C_a\cdots H_a$ bond that is being formed exhibits the characteristics of a weaker shared interaction. In addition, in Table 2 it can be observed that the C_a-H bonds in relation to the C_b-H bonds show significant differences in the topological local properties, reflecting the hybridization change of both carbon atoms (from $C_{(sp^2)}-H$ to $C_{(sp^3)}-H$ in an orbital scheme). All these results indicate the rupture of the olefin double bond and the formation of the carbenium ion in the transition state for the ethene protonation.

An electronic redistribution emerges and the bond's nature shows important features following a concerted mechanism in the acid site region: the bonds that are going to break themselves ($O_4\cdots H_a$) lose the characteristics of the shared interactions and acquire the characteristics of the closed shell interaction, whereas the $C_a\cdots H_a$ bond that is being formed shows topological characteristics of the shared interaction. Furthermore, the electronic redistribution over the region of the acid site is clearly seen by relief maps of $-\nabla^2\rho(r)$ (in Figure 4c) and will be are discussed later on.

On the other hand, the positive charge that appears on C_b (similar to the carbenium ion) interacts with one of the neighboring basic oxygen atoms of the zeolite (O_2) resulting in the formation of a new BCP corresponding to the $C_b\cdots O_2$ bond; it is clearly visualized in the molecular graph (Figure 2b). Also, Figure 4b shows a two-dimensional plot of $-\nabla^2\rho(r)$ in a $O_2C_bC_a$ plane. The topological properties at the $C_b\cdots O_2$ BCP (low value of density $\rho_b = 0.050$ au and the $|\lambda_1|/\lambda_3$ relationship $\ll 1$) are indicative of a weak electrostatic or ionic bond (closed shell interaction) with $\nabla^2\rho_b$ positive and $E_{e(b)}$ negative and near zero. The calculated $C_b\cdots O_2$ distance is significantly longer (2.121 Å) as well, suggesting that the interactions between the

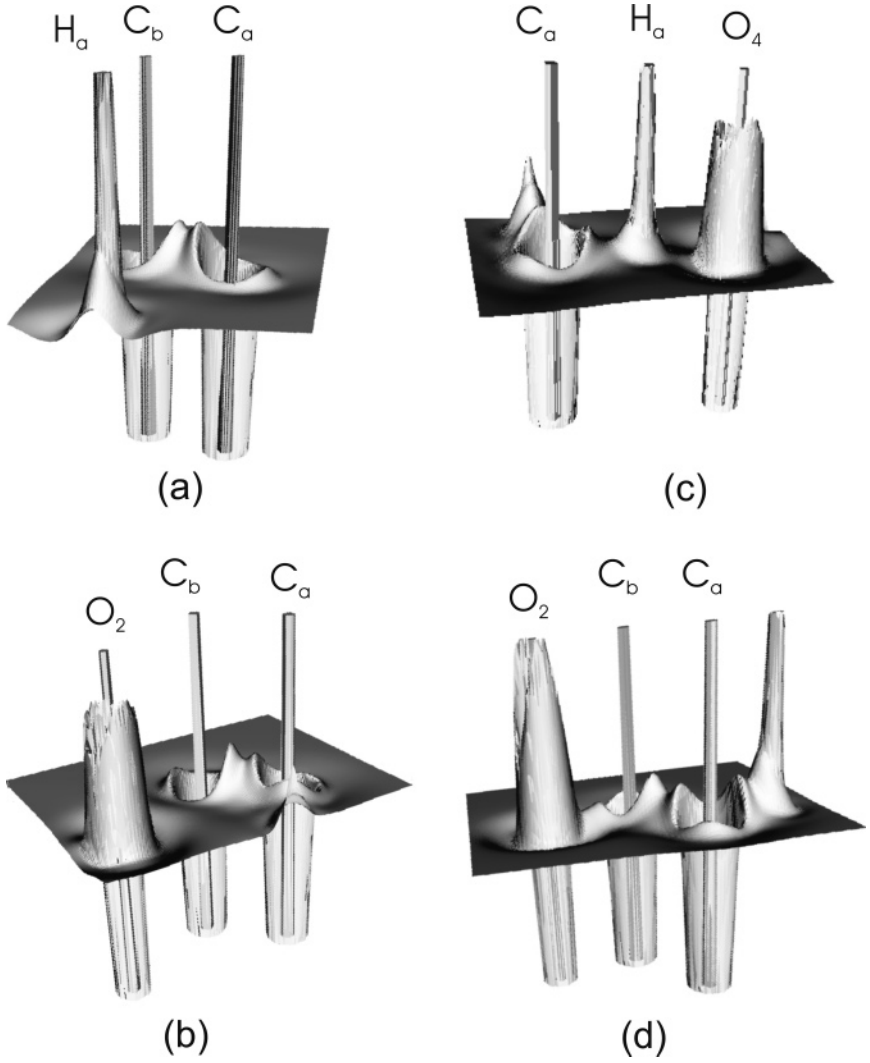

Figure 4. (a) Relief maps of the $-\nabla^2\rho(r)$ for ethene adsorbed, **3**, in a plane containing the $C_aC_bH_a$ atoms. Note the symmetry of the two maxima in the VSCC of the carbon atoms, along with the C_bC_a bond. (b and c) Relief maps of the $-\nabla^2\rho(r)$ for transition state, **4**, in the plane containing the $O_2C_bC_a$ atoms and in the plane containing the $C_aH_aO_4$ atoms. In part b, note the asymmetry between the two maxima indicated previously in Figure 4a (the highest maximum is always closer to the positively charged carbon atom). Also, in this figure the flatness of the distribution at the region of the O_2 atom in the direction of the C_b atom can be observed. (d) Relief maps of the $-\nabla^2\rho(r)$ for species **5**, in the plane containing the $O_2C_bC_a$ atoms. Other hydrogen atom (non-H_a) bonded to C_a is also included in the figure. In this figure, it is possible to appreciate the presence of a (3, −3) CP at the VS of C_b in the C_b-O_2 bond direction. Note that it is absent in Figure 4b.

positively charged C_b atom and the oxygen atom are not so strong in the transition state. The slight gain of the potential vs kinetic energy density at the BCP is indicative of a small degree of covalence in this new bond.

In summary, the AIM parameters for $C_b\cdots O_2$ and $H_a\cdots O_4$ bonds in the transition state (Table 2), show that they are not purely electrostatic and that the covalent character has considerably contributed to these bonds.

Other changes can be noted as well in the zeolite fragment. The $Al-O_2/Al-O_4$ bonds (involved in basic and acid sites) show a clear diminution/augmentation of the density and Laplacian at the BCPs; as a result, both BCPs in **4** then show similar characteristics.

1.3. Alkoxide Product. As pointed out above, a deeper analysis of the topological properties corresponding to BCPs in the bonding region defined by C_a, H_a, O_4 atoms (acid site) and C_b, O_2 atoms (basic site) is necessary in the transition state and alkoxide product. These facts are displayed in relief maps of the $-\nabla^2\rho(r)$ (see later).

Strong charge transfers from the lone pairs of the oxygen atom in the n^*C_b are expected, and the weak C−O bond formed in the course of the reaction (in the transition state) will be strengthened and shortened. The topological distribution of the electronic charge density at the C_b-O_2 BCP shows significant differences in species **4** and **5**. In the TS, it can be characterized as closed shell interactions with some covalent character, and in the alkoxide product, the increase of the charge density between the nuclei transform this interaction into a covalent bond or shared interaction, in which the Laplacian takes a negative value. In addition, the potential and kinetic energy densities are increased. Such an increase turns out to be greater in the potential energy. In accordance with these results, the relationship $|\lambda_1|/\lambda_3$ and the kinetic energy density by charge unit show an augmentation. Thus, the electronic charge density is accumulated between both atoms and then the alkoxide compound is stabilized. In addition, a closed shell interaction ($\rho_b = 0.006$ au and $\nabla^2\rho_b = 0.0213$ au with $|V_b| < G_b$) is detected between another hydrogen atom bonded to the C_a atom and the O_4, thus giving additional stabilization (indicated as $H_{11}\cdots O_4$ in Table 2).

As it was pointed out in previous papers related to Bader's theory, the interatomic interactions arise from a balance between

kinetic and potential energies or, in other words, from a balance between the concentration of the charge density (perpendicular contractions) along the bond path between the nuclei linked and the parallel expansion of ρ, with density being concentrated separately in each one of the atomic basins. If the Laplacian is negative, the contraction along the bond trajectory will show a local gain in the potential energy due to the increase of the charge density that is shared by both atoms. On the other hand, the $O_4\cdots H_a$ BCP is absent in the alkoxy product, reflecting the rupture of the weak bond between the H_a and O_4 atoms (present in the TS); subsequently, the H_a has been transferred totally.

In a shared interaction, electron density is both accumulated and concentrated along the bond path between the nuclei. However, it is important to highlight that the degree of accumulation of the charge density in the BCPs corresponding to the C_b-O_2 bond in the alkoxy product, **5** (measured by the value for ρ_b), and the extent of concentration of the density (measured by the magnitude of $\nabla^2\rho_b$) are diminished, with respect to another C−O bond taken as the reference.[33,44]

Recently, Pakiari and Eskandari[53] have established that another criterion must be taken into account to define the covalent character of the bonds. This means that along the bond path of covalent bonds, there must be a continuous region of space, including the valence region of the interacting atoms, in which the Laplacian is negative.[54] If the valence region of the atoms is separated by a region of space in which the Laplacian is positive, a contribution of an electrostatic (closed shell) interaction should be considered, although both $E_e(r)$ and $\nabla^2\rho(r)$ are negative at the BCP (see differences in relief maps (Figure 4b,d)).

However, in the catalytic fragment, in comparison to the change observed in the TS, the $Al-O_2/Al-O_4$ bonds emerge with different characteristics. This is a diminution/augmentation of ρ_b and $\nabla^2\rho_b$ at the BCPs, meaning that both BCPs in the alkoxy product show opposite tendencies to the adsorbed complex.

2. Relief Maps. Figure 4 (parts a−d) summarizes the results of the relief maps of $-\nabla^2\rho(r)$ for species **3**−**5** involved in the protonation reaction.

Figure 4a displays the relief map of $-\nabla^2\rho(r)$ for ethene adsorbed in the $H_aC_bC_a$ plane. The core and valence shell charge concentration can be seen at the position of each carbon atom. Also, coming first at the left of the figure, there is one maximum corresponding to the position of the hydrogen atom, H_a. In the C_a-C_b bond path, the two (3, −3) CPs corresponding to each valence shell (VS) of a carbon atom are highly symmetrical. These findings are additional evidence that the H_a atom is interacting symmetrically with both carbon atoms in ethene adsorbed.

In addition, the loss of the symmetry found in the C_a-C_b bond in ethene adsorbed can be clearly seen in the transition state, **4**, in Figure 4b. The core and valence shell charge concentration (VSCC) can be seen at the oxygen atom position. Note the surface flattened between the O_2 and C_b atoms, with (3, −3) CP absent in the VSCC at the C_b atom. In the $C_aH_aO_4$ plane, Figure 4c, the (3, −3) CP from the C_a atom in the direction of the H_a atom can be observed. Take notice of the electronic density over the plane surface of the figure in the $H_a\cdots O_4$ direction.

In Figure 4d, the relief map of $-\nabla^2\rho(r)$ for the alkoxy product in the $O_2C_bC_a$ plane is shown. In addition, another hydrogen atom (bonded to C_a) is slightly out of the plane. However, the presence of the charge concentration CP at the C_a atom in the direction of this hydrogen atom can be observed. On the other hand, note the emergence of the maximum in the VSCC of the C_b in the C_b-O_2 direction while it is absent in the transition state (see Figure 4b).

As mentioned above, the effect of the positive charge that appears on C_b (similar to the carbenium ion) in the concerted mechanism of the protonation of ethene is also appreciated in the relief map of $-\nabla^2\rho(r)$ (see Figure 4b). In the transition state, it is possible to appreciate how the highest maximum is much closer to the C_b atom. This result is in accordance with the displacement of the charge concentration toward the more positively charged atom in the relief map.[55]

3. Topological Atomic Properties. The ability to determine the individual atomic contributions to the changes in charge, energy, and volume (characteristic of a given chemical reaction) should be of particular use for obtaining a better understanding of the atomic interactions between fragments in reaction sites. With the use of the topology of the electron density, the atoms in molecules theory defines an atom as a bounded portion of real space, known as the atomic basin, denoted by Ω. In this theory, all information about a particular AIM atom is contained in its finite volume and the properties can be obtained by integrating the corresponding property density over the atomic basin.[33,56] In addition, atomic properties, defined by AIM as integrations over the atomic volume, can be computed from experimental electron density.[57]

In Table 4, the topological atomic properties of selected atoms in the site of the reaction are shown.

In the present work, the atomic properties are the average number of electrons, $N(\Omega)$, from which the atomic net charge, $q(\Omega)$, can be calculated as $Z_\Omega - N(\Omega)$, with Z_Ω being the nuclear charge of the atom; the atomic energy, $E(\Omega)$; the atomic volume, $v(\Omega)$; and the first moment of the atomic charge distribution, $M(\Omega)$. This last property measures the extent and direction of the dipolar polarization undergone by the atomic density.

At the beginning of the reaction, in the π-complex or adsorbed species, the electronic populations of the C_a and the C_b atoms are similes. The atomic volumes, the electronic energies, and the dipolar polarizations do not show significant differences.

The changes in electronic distribution that take place on the σ and π bonds for the formation of the transition state in a concerted mechanism are mirrored by the atomic properties. The C_a-C_b bond in the transition state undergoes a transition from a double to a single bond. Therefore, the electronic charge density is shifting toward the carbon atom bonded to the electrophilic proton that is being transferred from the acid site. The formation of the ionic transition state, by concerted mechanism, is clearly reflected in the atomic charges. In the moiety $O_4\cdots H_a\cdots C_a-C_b\cdots O_2$, the atomic charge takes on values of: −1.549 au, +0.414 au, −0.110 au, + 0.116 au, and −1.544 au, respectively. In accordance with the proposed ionic mechanism, these results show that both carbon atoms have opposite charges, the hydrogen atom has an important positive charge and the oxygen atoms have a similar negative charge.

In the course of the reaction, the change of the properties are analyzed by taking into consideration the difference in the atomic property in the the TS with respect to the adsorbed complex, $\Delta_{(TS-Ads)}$, and in the alkoxide product with respect to the TS, $\Delta_{(Alk-TS)}$.

The only atoms whose populations are affected significantly when passing from the adsorbed to the transition state (i.e., the absolute difference is greater than 0.02 *e*) are C_b which loses 0.149 *e*, H_a which gains 0.214 *e*, and O_4 which gains 0.025 *e* after sharing its hydrogen with the carbon C_a.

TABLE 4: Topological Atomic Properties of Selected Atoms in Species 3, 4, and 5 Species[a]

atom	species	$N(\Omega)$	$E(\Omega)$	$q(\Omega)$	$v(\Omega)$	$\|M(\Omega)\|$
C_a						
	3	6.0318	−37.8456	−0.0318	89.9325	0.0770
	4	6.1101	−37.8986	−0.1101	79.3930	0.3255
	5	5.9188	−37.8096	+0.0812	67.9295	0.0812
C_b						
	3	6.0330	−37.8471	−0.0330	89.9680	0.0806
	4	5.8836	−37.7883	+0.1164	71.2958	0.1845
	5	5.5430	−37.5709	+0.4570	52.7117	0.5374
H_{10}						
	3	0.9530	−0.6048	+0.0470	47.7972	0.1129
	4	0.9693	−0.6091	+0.0307	47.5303	0.1245
	5	0.9726	−0.6133	+0.0274	46.9408	0.1174
H_a						
	3	0.3723	−0.3129	+0.6277	17.0022	0.1480
	4	0.5865	−0.4152	+0.4135	17.4228	0.0243
	5	1.0136	−0.6280	−0.0136	50.4208	0.1310
O_2						
	3	9.6794	−75.5434	−1.6794	142.8426	0.2403
	4	9.5441	−75.4796	−1.5441	114.7843	0.4765
	5	9.4210	−75.5577	−1.4210	93.9955	0.3201
O_4						
	3	9.5249	−75.5893	−1.5249	118.1328	0.1570
	4	9.5485	−75.5261	−1.5485	118.4145	0.3784
	5	9.6808	−75.5458	−1.6808	142.4563	0.2076
O_6						
	3	9.6805	−75.5458	−1.6805	143.7930	0.2032
	4	9.6783	−75.5403	−1.6783	144.1234	0.1876
	5	9.6802	−75.5460	−1.6802	141.6515	0.2015
O_7						
	3	9.6837	−75.5442	−1.6837	137.8965	0.2776
	4	9.6787	−75.5469	−1.6787	143.0225	0.2008
	5	9.6764	−75.5485	−1.6764	132.9094	0.3087
Al_3						
	3	10.4386	−241.8201	+2.5614	27.4031	0.0456
	4	10.4414	−241.8209	+2.5586	26.9435	0.0301
	5	10.4406	−241.8228	+2.5594	27.3228	0.0107
Si_1						
	3	10.9972	−288.7945	+3.0028	34.0507	0.0841
	4	11.0234	−288.8131	+2.9766	34.4607	0.0827
	5	11.0569	−288.8028	+2.9431	36.1910	0.1117
Si_5						
	3	11.0381	−288.8082	+2.9619	34.9211	0.0992
	4	11.0248	−288.8096	+2.9752	35.3330	0.0849
	5	10.9970	−288.7942	+3.0030	33.9223	0.0805

[a] Atomic electron populations $N(\Omega)$, the atomic energies $E(\Omega)$, net atomic charge $q(\Omega)$, atomic volume integrated to the 0.001 au isodensity envelope, $v(\Omega)$, and atomic dipolar moment $|M(\Omega)|$ (all values in au). 1 au (μ) = 8478 × 10^{-30} C m; 1 au (V, E) = 2.6255 kJ mol^{-1}.

The carbon atom C_a experiences a slight increase (0.078 *e*) in population, and hence, it is already 3.5 times more negative after protonation (from $q_{(\Omega)} = -0.032$ au in the adsorbed to −0.110 au in the TS). It achieves this increase in population by extracting electrons from the neighboring C_b (disruption of the double bond), forcing the electropositive carbon C_b ($q_{(\Omega)} = +0.116$ au in the TS) to bear the increase in the positive charge on the O_2 (basic site). Thus, the oxygen atom in the basic site loses 0.135 *e*.

In other words, the destabilization in the transition state of the ethene protonation reaction is mostly localized at the ionized atoms and their immediate neighborhood. As a consequence of the augmentation of the electronic population, the H_a and C_a atoms are stabilized but the C_b atom and both oxygens from the acid and basic sites are destabilized in the transition state.

It is necessary to have in mind that in this new situation, both carbon atoms share a new interatomic surface, the C_a with the H_a that it is being transferred from the acid site and, on the other hand, the C_b atom with the oxygen atom of the basic site.

TABLE 5: Natural Charge Calculated at the B3LYP/6-31G Level of Theory**[a]

atom	**1**	**2**	**3**	**4**	**5**
C_a	−0.4347		−0.4560	−0.8088	−0.7247
C_b	−0.4347		−0.4580	−0.0873	−0.0997
H_a		+0.5585	+0.5548	+0.4344	+0.2384
O_2		−1.3021	−1.3004	−1.1886	−0.9625
O_4		−1.1151	−1.1370	−1.2180	−1.3031
O_6		−1.3009	−1.3017	−1.3023	−1.3037
O_7		−1.2979	−1.2999	−1.2987	−1.2999
Al_3		+2.0538	+2.0619	+2.0733	+2.0704
Si_1		+1.2819	+1.2870	+1.2427	+1.2284
Si_5		+1.2280	+1.2338	+1.2517	+1.2888

[a] In au.

In both carbons, an important volume diminution ($\Delta v_{(\Omega)(TS-Ads)} = -10.54$ au in C_a and −18.67 au in C_b) and an augmentation of first moment ($\Delta|M_{(\Omega)}|_{(TS-Ads)} = 0.249$ au in C_a and 0.104 au in C_b) are observed. The first effect is more outstanding in the C_b atom and the second one in the C_a atom. The volume variations over the H_a and O_4 atoms are slightly significant, but the greatest diminution in atomic volume is observed in the oxygen atom of the basic site ($\Delta v_{(\Omega)(TS-Ads)} = -28.06$ au). This atom, as well as the C_a atom, shows the highest increases of the first moment ($\Delta|M_{(\Omega)}|_{(TS-Ads)} = 0.236$ au in O_2 and 0.249 au in C_a).

The situation again changes when forming the alkoxide product. Some present changes in the TS follow the same tendency, but they are more pronounced, for example: the loss of electronic population in O_2 and the increase of the same one in O_4 and in H_a. Along with the formation of the C_b-O_2 bond, both carbon atoms undergo an electronic redistribution in the alkoxide complex, with a dramatic volume decrease at the C_b atom and a slighter electronic population decrease. This situation is minimal in C_a and shows the difference in both carbon atoms. Now, the C_a is bonding to three hydrogen atoms and C_b is bonding to two hydrogen atoms and an oxygen atom in the alkoxide compound. As it was expressed above, these decreases/increases of $N_{(\Omega)}$ are accompanied by important decreases/increases of the atomic volume. Thus, it is observed that the O_2 ($v_{(\Omega)} = 93.99$ au; $\Delta v_{(\Omega)(Alk-TS)} = -20.79$ au); C_b ($v_{(\Omega)} = 52.71$ au ; $\Delta v_{(\Omega)(Alk-TS)} = -18.59$ au); and C_a ($v_{(\Omega)} = 67.93$ au; $\Delta v_{(\Omega)(Alk-TS)} = -11.46$ au) atoms become very compact in the alkoxide product by volume contraction (in the order of $O_2 > C_b \gg C_a$). In comparison to this situation, the H_a and O_4 atoms become more diffuse by volume expansion. An important increase of the atomic population and the atomic volume are observed at H_a ($N_{(\Omega)} = 1.0136$ au ; $\Delta N_{(\Omega)(Alk-TS)} = 0.4271$ au; and $v_{(\Omega)} = 50.42$ au ; $\Delta v_{(\Omega)(Alk-TS)} = 33.0$ au). This also takes place but in a less considerable magnitude at O_4 ($v_{(\Omega)} = 142.46$ au ; $\Delta v_{(\Omega)(Alk-TS)} = 23.04$ au). The atomic properties of H_a in the alkoxy product exhibit the characteristic of a hydrogen atom bonding to a $C(sp^3)$ atom.

On the other hand, the stabilization of the alkoxy product is mirrored by the $E(\Omega)$ values; an important augmentation of the stability is observed in the H_a and O_2 atoms as well as a slight augmentation observed in O_4. In the last two atoms, it is accompanied by a diminution of the dipolar polarization in the alkoxide product.

Finally, in the course of the reaction the Al atom and the Si atoms show smaller variation in their properties.

4. Natural Populations Analysis. The natural charges (q) obtained by natural population analysis (NPA) are summarized in Table 5. The results obtained along the reaction show tendencies similar to the $q(\Omega)$ values obtained by AIM analysis.

They indicate the magnitudes of the negative qO_2/O_4 and the positive qSi_1/Si_5 decrease/increase from ethene adsorbed, **3**, to the alkoxy product, **5**. In ethene adsorbed, the negative $qC_{a,b}$ and positive qH_a values augment slightly with respect to the isolated species, whereas in the transition state, an abrupt charge separation, reflecting the rupture of the olefin double bond and the formation of the carbenium ion, is observed. At the same time, the proton-transfer degree is mirrored by qH_a. As it was expressed previously, the hydrogen atom bonded at O_4 interacts with both carbon atoms in the π-complex, **3**; this atom is dicoordinated in **4** and in **5**, it is bonded to the carbon atom more negatively charged, C_a.

To conclude, the global analysis of the NPA results reveals that the charges obtained by AIM analysis are more descriptive of the change produced in the course of the reaction. For example, in the TS, the atomic charge magnitude for the C_a and C_b atoms are very similar and of opposite signs, whereas in NPA both atoms show different magnitudes (they differ in an order of magnitude) but they exhibit the same sign.

Conclusions

A topological study of the reactants, ethene adsorbed, transition state, and alkoxide product involved in the ethene protonation reaction catalyzed by acidic zeolite is accomplished in this work within the framework of the density functional theory and the atoms in molecules theory. All the topological features show the bifunctional character of the catalytic site in the protonated zeolite.

In the presence of ethene, the acidic hydrogen atom in the protonated zeolite (with diminished electronic population and positively charged) acts as a true electrophile over the π-cloud of the ethenic fragment. Thus, the oxygen atom bearing the hydrogen atom in the protonated zeolite (T5-OH cluster) acts as a Brønsted acid, whereas the other oxygen atom (with greater electronic population, basic site) plays the role of a Lewis base. A continuous diminution of their electronic population (due to electron donation) and their size are observed at the O_2 atom along the reaction pathway.

The characteristic topological feature of the electron density in this process is the electron charge density delocalization, which is spread over the nuclei localized principally in the moiety ($O_4\cdots H_a\cdots C_a-C_b\cdots O_2$). The average atomic properties clearly show the change these atoms undergo along the course of the reaction. In accordance with other authors, it is found that no free carbenium ion is presented in the course of the ethene protonation reaction.

The molecular graphs obtained for the different species agree with the proposed structures, with an acidic hydrogen atom originally linked by a short bond path to an O_4 atom in the isolated species (acid site). In the adsorbed ethene, **3**, this BP is lengthened and a new and extended BP emerges with a direction to the middle C_a-C_b bond; then the acidic atom is linked by longer BPs to the C_a and O_4 atoms in **4** and by a shorter BP only to the C_a atom in **5**. Finally, the acidic proton has been transferred totally, and the zeolite is deprotonated. In the basic site region, a long BP links the positively charged C_b atom from the ethene fragment to the oxygen atom in **4** and this BP is shorter in **5**.

The analysis of the topological parameters in the BCPs of all the bond paths, in the TS, shows that the hydrogen atom from the acid site in protonated zeolite is connected to the carbon by a covalent bond with some contribution of an electrostatic interaction and to the oxygen atom by a closed shell interaction with some contribution of covalent character.

In conclusion, in the transition state, the dominant interactions are partially electrostatic and partially covalent in nature. The covalent contribution increases as *the concentration and accumulation of the charge density* along the bond path between the nuclei linked increases.

The ionic character of the transition state is evident in the atomic charge on each carbon atom. The global analysis of the NPA results reveals that the average atomic charges obtained by AIM analysis are more descriptive of the change produced in the course of the reaction.

Finally, it is found that a better understanding of the ethene protonation reaction is obtained when the topological properties of the bifunctional sites on the zeolite and over the atoms of the organic fragment are analyzed from local and average atomic properties. The analysis of the average atomic energy in the different atoms clearly reflect the energetic destabilization in the cyclic transition state and how they bring about the stabilization in the alkoxy product.

Certainly, in the catalyzed reaction by zeolite, the debate question is centered on the formation of the alkoxy products or free carbenium ion and the topological study of the C_b-O bonds on the reaction path shows interesting results about this question. The alkoxy product is formed as a consequence of the electrophilic strength developed by the positively charged C_b atom; this atom withdraws electrons from the atomic basin of the (basic) O_2 atom, which acts as Lewis basic site. Then, if the charge can be delocalized or spread over other σ C−C or C−H bonds in the organic fragment in bulky species, then the electrophilic strength of the C_b atom for the C_b-O interaction is diminished and the free carbocation can be formed. It is interesting to highlight that it is a key electronic effect. The process by which the C_b atom withdraws electrons from their neighboring atoms is mirrored by the local and atomic topological properties. In this reaction, the C_b-O_2 bond formed in the alkoxy product can be defined as a *weaker shared interaction*. The strength of the bonds is directly related to the accumulation of charge density at the BCP, and we think that if the density at the BCP is diminished with respect to other C−O bonds, then the C_b-O_2 bond in the ethoxy compound will be more easily broken, or in other words it will have a lower energetic requirement to break itself.

The present results suggest that a deep knowledge of the topological characteristic of the charge density distribution and of the Laplacian distribution in these bonds is necessary for the understanding of the stability of the bulky alkoxide species or the bulky carbenium ion in a specific reaction. These facts are under investigation in our laboratory (in a series of olefins of greater size), and results will be published in the near future.

Acknowledgment. The authors acknowledge to the SECYT UNNE and SECYT UTN-FRRe for financial support. M.F.Z. is a fellow of CONICET, and N.M.P. is career researcher of CONICET, Argentina.

References and Notes

(1) Corma, A. *Chem. Rev.* **1995**, *95*, 559.

(2) (a) Olah, G. A.; Prakash, S. K.; Williams, R. E.; Field, L. D.; Wade, K. In *Hydrocarbon Chemistry*; Wiley-Interscience: New York, 1987. (b) Olah, G. A. *Carbocations and Electrophilic Reaction*; Wiley: NewYork, 1973.

(3) Kiricsi, I.; Förster, H.; Tasi, G.; Nagy, J. B. *Chem. Rev.* **1999**, *99*, 2085.

(4) (a) Tal'roze, V. L.; Lyubimova, A. K. *Dokl. Akad. Nauk. SSSR* **1952**, *86*, 909. (b) Olah, G. A. *J. Am. Chem. Soc.* **1972**, *94*, 808.

(5) Okulik, N. B.; Peruchena, N. M.; Jubert, A. H. *J. Phys. Chem. A* **2006**, *110*, 9974 and references therein.

(6) Kazansky, V. B. *Catal. Today* **1999**, *51*, 419.

(7) Boronat, M.; Zicovich-Wilson, C. M.; Viruela, P.; Corma, A. *J. Phys. Chem. B* **2001**, *105*, 11169.
(8) Boronat, M.; Viruela, P. M.; Corma, A. *J. Am. Chem. Soc.* **2004**, *126*, 3300.
(9) Rigby, A. M.; Kramer, G. J.; van Santen, R. A. *J. Catal.* **1997**, *170*, 1.
(10) Sinclair, P. E.; de Vries, A.; Sherwood, P.; Catlow, C. R. A.; van Santen, R. A. *J. Chem. Soc., Faraday Trans.* **1998**, *94*, 3401.
(11) Rozanska, X.; van Santen, R. A.; Demuth, T.; Hutschka, F.; Hafner, J. *J. Phys. Chem. B* **2003**, *107*, 1309.
(12) Kazansky, V. B. *Acc. Chem. Res.* **1991**, *24*, 379.
(13) Correa, R. J.; Mota, C. J. A. *Phys. Chem. Chem. Phys.* **2002**, *4*, 375.
(14) (a) Kazansky, V. B.; Frash, M. V.; van Santen, R. A. *Appl. Catal. A: General* **1996**, *146*, 225. (b) Rigby, A. M.; Frash, M. V. *J. Mol. Catal. A: Chem.* **1997**, *126*, 61.
(15) Viruela, P.; Zicovich-Wilson, C. M.; Corma, A. *J. Phys. Chem. B* **1993**, *97*, 13713.
(16) Boronat, M.; Viruela, P.; Corma, A. *J. Phys. Chem. A* **1998**, *102*, 982.
(17) Boronat, M.; Zicovich-Wilson, C. M.; Viruela, P.; Corma, A. *Chem.—Eur. J.* **2001**, *7*, 1295.
(18) Rozanska, X.; Demuth, T.; Hutschka, F.; Hafner, J.; van Santen, R. A. *J. Phys. Chem. B* **2002**, *106*, 3248.
(19) Sauer, J.; Ugliengo, P.; Garrone, E.; Saunders, V. R. *Chem. Rev.* **1994**, *94*, 2095.
(20) Okulik, N. B.; Pis Diez, R.; Jubert, A. H. *J. Phys. Chem. A* **2003**, *107*, 6225.
(21) Okulik, N. B.; Pis Diez, R.; Jubert, A. H.; Esteves, P. M.; Mota, C. J. A. *J. Phys. Chem. A* **2001**, *105*, 7079.
(22) Okulik, N. B.; Pis Diez, R.; Jubert, A. H. *J. Phys. Chem. A* **2004**, *108*, 2469.
(23) Milas, I.; Nascimento, M. A. C. *Chem. Phys. Lett.* **2001**, *338*, 67.
(24) Svelle, S.; Arstad, B.; Kolboe, S.; Swang, O. *J. Phys. Chem. B* **2003**, *107*, 9281.
(25) Arstad, B.; Kolboe, S.; Swang, O. *J. Phys. Chem. B* **2002**, *106*, 12722.
(26) Svelle, S.; Kolboe, S.; Swang, O. *J. Phys. Chem. B* **2003**, *107*, 5251.
(27) Svelle, S.; Kolboe, S.; Swang, O. *J. Phys. Chem. B* **2004**, *108*, 2953.
(28) Nieminen, V.; Sierka, M.; Yu Murzin, D.; Sauer, J. *J. Catal.* **2005**, *231*, 393.
(29) Ugliengo, P.; Ferrari, A. M.; Zecchina, A.; Garrone, E. *J. Phys. Chem.* **1996**, *100*, 3632.
(30) Okulik, N. B.; Peruchena, N.; Esteves, P. M.; Mota, C. J. A.; Jubert, A. H. *J. Phys. Chem. A* **2000**, *104*, 7586.
(31) Okulik, N. B.; Peruchena, N. M.; Esteves, P.; Mota, C.; Jubert, A. H. *J. Phys. Chem. A* **1999**, *103*, 8491.
(32) Okulik, N. B.; Sosa, G. L.; Esteves, P.; Mota, C.; Jubert, A. H.; Peruchena, N. M. *J. Phys. Chem. A* **2002**, *106*, 1584.
(33) Bader, R. F. W. *Atoms in Molecules. A Quantum Theory*; Oxford Science Publications, Clarendon Press: London, 1990.
(34) Corma, A.; Garcia, H.; Sastre, G.; Viruela, P. *J. Phys. Chem. B* **1997**, *101*, 4575.
(35) (a) Becke, A. D. *J. Chem. Phys.* **1993**, *98*, 5648. (b) Lee, C.; Yang, W.; Parr, R. G. *Phys. Rev. B* **1988**, *37*, 785.
(36) Frisch, M. J.; Trucks, G. W.; Schlegel, H. B.; Scuseria, G. E.; Robb, M. A.; Cheeseman, J. R.; Montgomery, J. A., Jr.; Vreven, T. ; Kudin, K. N.; Burant, J. C.; Millam, J. M.; Iyengar, S. S.; Tomasi, J.; Barone, V.; Mennucci, B.; Cossi, M.; Scalmani, G.; Rega, N.; Petersson, G. A.; Nakatsuji, H.; Hada, M.; Ehara, M.; Toyota, K.; Fukuda, R.; Hasegawa, J.; Ishida, M.; Nakajima, T.; Honda, Y.; Kitao, O.; Nakai, H.; Klene, M.; Li, X.; Knox, J. E.; Hratchian, H. P.; Cross, J. B.; Adamo, C.; Jaramillo, J.; Gomperts, R.; Stratmann, R. E.; Yazyev, O.; Austin, A. J.; Cammi, R.; Pomelli, C.; Ochterski, J. W.; Ayala, P. Y.; Morokuma, K.; Voth, G. A.; Salvador, P.; Dannenberg, J. J.; Zakrzewski, G.; Dapprich, S.; Daniels, A. D.; Strain, M. C.; Farkas, O.; Malick, D. K.; Rabuck, A. D.; Raghavachari, K.; Foresman, J. B.; Ortiz, J. V.; Cui, Q.; Baboul, A. G.; Clifford, S.; Cioslowski, J.; Stefanov, B. B.; Liu, G.; Liashenko, A.; Piskorz, P.; Komaromi, I.; Martin, R. L.; Fox, D. J.; Keith, T.; Al-Laham, M. A.; Peng, C. Y.; Nanayakkara, A.; Challacombe, M.; Gill, P. M. W.; Johnson, B.; Chen, W.; Wong, M. W.; Gonzalez, C.; Pople, J. A. *Gaussian 03*, revision D.01; Gaussian, Inc.: Wallingford, CT, 2004.
(37) Schlegel, H. B. *J. Comput. Chem.* **1982**, *3*, 214.
(38) Gonzalez, C.; Schlegel, H. B. *J. Chem. Phys.* **1989**, *90*, 2154.
(39) Gonzalez, C.; Schlegel, H. B. *J. Phys. Chem.* **1990**, *94*, 5523.
(40) Bader, R. F. W. *AIMPAC*; a suite of programs for the Theory of Atoms in Molecules; McMaster University: Hamilton, Ontario, Canada.
(41) Blieger-König, F.; Schönbohn, J. *AIM2000* program package, version 2.0; chemical adviser Bader, R. F. W.; Büro fur Innovative Software Streibel Biegler-König: Germany, 2002.
(42) Blieger-König, F.; Bader, R. F. W.; Tang, T. H. *J. Comput. Chem.* **1982**, *3*, 317.
(43) Glendening, E. D.; Reed, A. E.; Carpenter, J. E.; Weinhold, F. *NBO*, version 3.1; University of Wisconsin: Madison, WI.
(44) Popelier, P. L. A. *Atoms in Molecules. An Introduction*; Pearson Education: Harlow, U.K., 2000.
(45) Bader, R. F. W. *J. Phys. Chem. A* **1998**, *102*, 7314.
(46) Bader, R. F. W.; Nguyen-Dang, T. T.; Tal, Y. *Rep. Prog. Phys.* **1981**, *44*, 893.
(47) Jenkins, S.; Morrison, I. *Chem. Phys. Lett.* **2000**, *317*, 97.
(48) (a) Popelier, P. L. A. *Coord. Chem. Rev.* **2000**, *197*, 169. (b) Lobayan, R. M.; Sosa, G. L.; Jubert, A. H.; Peruchena, N. M. *J. Phys. Chem. A* **2004**, *108*, 4347.
(49) Gillespie, R. J. *Struct. Chem.* **1998**, *9*, 73.
(50) Gillespie, R. J. *Can. J. Chem.* **1992**, *70*, 742.
(51) Novoa, J. J.; Mota, F. *Chem. Phys. Lett.* **2000**, *318*, 345.
(52) Collard, K.; Hall, G. G. *Int. J. Quantum Chem.* **1977**, *12*, 623.
(53) Pakiari, A. H.; Eskandari, K. *J. Mol. Struct.: THEOCHEM* **2006**, *759*, 51.
(54) Koritsanszky, T. S.; Coppens, P. *Chem. Rev.* **2001**, *101*, 1583.
(55) Lobayan, R. M.; Sosa, G. L.; Jubert, A. H.; Peruchena, N. M. *J. Phys. Chem. A* **2005**, *109*, 181.
(56) Blieger-König, F. *J. Comput. Chem.* **2000**, *21*, 1040.
(57) Koritsanszky, T.; Flaig, R.; Zobel, D.; Krane, H. G.; Morgenroth, W.; Luger, P. *Science* **1998**, *279*, 356.